Larger value for H_0 by an evolving gravitational constant

Matteo Braglia,[1,2,3,*] Mario Ballardini,[1,2,3,4,†] William T. Emond,[5,‡] Fabio Finelli,[2,3,§]
A. Emir Gümrükçüoğlu,[6,∥] Kazuya Koyama,[6,¶] and Daniela Paoletti[2,3,**]

[1]*Dipartimento di Fisica e Astronomia, Alma Mater Studiorum Università di Bologna,*
Via Gobetti, 93/2, I-40129 Bologna, Italy
[2]*INAF/OAS Bologna, via Gobetti 101, I-40129 Bologna, Italy*
[3]*INFN, Sezione di Bologna, Via Berti Pichat 6/2, I-40127 Bologna, Italy*
[4]*Department of Physics and Astronomy, University of the Western Cape, Cape Town 7535, South Africa*
[5]*School of Physics and Astronomy, University of Nottingham, University Park,*
Nottingham NG7 2 RD, United Kingdom
[6]*Institute of Cosmology and Gravitation, University of Portsmouth,*
Dennis Sciama Building, Portsmouth PO1 3FX, United Kingdom

We provide further evidence that a massless cosmological scalar field with a nonminimal coupling to the Ricci curvature of the type $M_{pl}^2(1 + \xi\sigma^n/M_{pl}^n)$ alleviates the existing tension between local measurements of the Hubble constant and its inference from cosmic microwave background anisotropies and baryonic acoustic oscillations data in the presence of a cosmological constant. In these models, the expansion history is modified compared to ΛCDM at early time, mimicking a change in the effective number of relativistic species, and gravity weakens after matter-radiation equality. Compared to ΛCDM, a quadratic ($n = 2$) coupling increases the Hubble constant when Planck 2018 (alone or in combination with BAO and SH0ES) measurements data are used in the analysis. Negative values of the coupling, for which the scalar field decreases, seem favored and consistency with the Solar System can be naturally achieved for a large portion of the parameter space without the need of any screening mechanism. We show that our results are robust to the choice of n, also presenting the analysis for $n = 4$.

I. INTRODUCTION

Despite its simplicity, the six parameters Λ cold dark matter (CDM) concordance model has been extremely successful in explaining cosmic microwave background (CMB) anisotropies, baryon acoustic oscillations (BAOs), the abundance of primordial light element by big bang nucleosynthesis (BBN), luminosity distance of type Ia supernovae (SNe Ia), and several other cosmological observations. However, the unknown nature of the dark energy (DE) and CDM permeating our Universe justifies the search for other alternatives. These doubts have been recently corroborated by growing discrepancies between the present rate of the expansion of the Universe H_0 inferred from CMB anisotropies measurements and the one estimated by low-redshift distance-ladder measurements [1].

The value of the Hubble constant inferred from Planck 2018 data, $H_0 = (67.36 \pm 0.54)$ km s^{-1} Mpc^{-1} [2], is in a 4.4σ tension with the most recent distance-ladder measurement from the SH0ES team [3], $H_0 = (74.03 \pm 1.42)$ km s^{-1} Mpc^{-1}, determined by using Cepheid-calibrated SNe Ia with new parallax measurements from Hubble Space Telescope (HST) spatial scanning [4]. This is a recent snapshot of a long-standing tension of distance-ladder measurements of H_0 with a much wider set of cosmological data rather than Planck data only [5], whose magnitude is possibly affected by unaccounted effects such as uncertainties in calibration [6–9] or in the luminosity functions of SNIa [6–11]. Other determinations of H_0 at low redshift, such as from strong-lensing time delay [12], also point to a higher H_0 than the one inferred by Planck data.

Assuming that this H_0 *tension* is not due to unknown systematics or unaccounted effects as those mentioned above, some new physics is therefore needed to solve it. One way to address the tension is to modify early time (for redshifts around matter-radiation equality) physics in order to reduce the inferred value of the comoving sound horizon at baryon drag r_s. Indeed, a smaller value of the comoving sound horizon at baryon drag r_s can provide a higher value

*matteo.braglia2@unibo.it
†mario.ballardini@inaf.it
‡william.emond@nottingham.ac.uk
§fabio.finelli@inaf.it
∥emir.gumrukcuoglu@port.ac.uk
¶kazuya.koyama@port.ac.uk
**daniela.paoletti@inaf.it

of H_0 without spoiling the fit to CMB anisotropies data and changing the BAO observables [13–15]. A prototypical example of such an early time modification is an excess in the number N_{eff} of relativistic degrees of freedom, eventually interacting with hidden dark sectors [16–25].

An alternative solution to N_{eff}, which can substantially alleviate the tension, consists in early dark energy (EDE) models [26–31]. In these models, a scalar field minimally coupled to gravity is subdominant and frozen by the Hubble friction at early times and starts to move around the matter-radiation equality when its effective mass becomes comparable to the Hubble flow and quickly rolls to the minimum of its potential, injecting an amount of energy in the cosmic fluid sharply to sizably reduce r_s. The parameters of the potential and the initial value of the scalar field, which can be remapped in the critical redshift at which the scalar field moves z_c and the maximum value of the energy injection $\Omega_\phi(z_c)$, have to be fine-tuned to successfully ease the Hubble tension.[1]

In this paper, we study the capability of a massless scalar field σ with a nonminimal coupling of the form $F(\sigma) = M_{\text{pl}}^2[1 + \xi(\sigma/M_{\text{pl}})^n]$, where $M_{\text{pl}} = 1/\sqrt{8\pi G} = 2.435 \times 10^{18}$ GeV is the reduced Planck mass, and n is taken as an even and positive integer, to reduce the H_0 tension. This simple model relies on the degeneracy between a nonminimal coupling to the Ricci curvature and the Hubble parameter which has been studied in previous works on the constraints on scalar-tensor theories of gravity[2] [35–38]. In general, scalar-tensor models modify both the early (in a way that resembles a contribution of an extra *dark* radiation component) and late-time expansion of the Universe [37]. By our embedding of a massless σ in ΛCDM, we focus on the early type of modification in this paper. In the case of a negative coupling $\xi < 0$, the scalar field decreases because of the coupling to matter, leading to cosmological post-Newtonian parameters which can be naturally consistent with the Solar System constraints $\gamma_{\text{PN}} - 1 = (2.1 \pm 2.3) \times 10^{-5}$ at 68% CL [39] and $\beta_{\text{PN}} - 1 = (4.1 \pm 7.8) \times 10^{-5}$ at 68% CL [40], extending what already emphasized for a conformal coupling (CC, i.e., $\xi = -1/6$) in [37]. We also investigate to the case where N_{eff}, which describes the effective number of relativistic species, is included in the analysis.

This paper is organized as follows. In Sec. II, we describe the background evolution of the model and compare it to other existing solutions to the H_0 tension. We describe the data sets and the details of our Markov-chain Monte Carlo (MCMC) analysis in Sec. III and present our results in Sec. IV. We end by discussing our results in Sec. V.

II. BACKGROUND EVOLUTION

The model that we consider is described by the action

$$S = \int d^4x \sqrt{-g}\left[\frac{F(\sigma)}{2}R + \frac{(\partial\sigma)^2}{2} - \Lambda + \mathcal{L}_m\right], \quad (1)$$

where $F(\sigma) := M_{\text{pl}}^2[1 + \xi(\sigma/M_{\text{pl}})^n]$ is the nonminimal coupling (NMC) of the scalar field to the Ricci scalar R, $(\partial\sigma)^2 := g^{\mu\nu}\partial_\mu\sigma\partial_\nu\sigma$, $\mathcal{L}_m$ is the Lagrangian density describing the matter sector, and M_{pl}, Λ are the reduced Planck mass and bare cosmological constant, respectively. The $n = 2$ case has been studied in Refs. [37,41] with a potential $V \propto F^2$, which is, however, close to a flat potential for the range of ξ allowed by observations.[3]

The Friedmann and the Klein-Gordon equations in the spatially flat Friedmann-Lemaitre-Robinson-Walker (FLRW) background are given by

$$3FH^2 = \rho + \frac{\dot{\sigma}^2}{2} + \Lambda - 3\dot{F}H$$
$$:= \rho + \rho_\sigma, \quad (2a)$$

$$\ddot{\sigma} + 3H\dot{\sigma} = \frac{F_{,\sigma}}{2F + 3F_{,\sigma}^2}[\rho - 3p + 4\Lambda - (1 + 3F_{,\sigma\sigma})\dot{\sigma}^2], \quad (2b)$$

where $\rho(p)$ collectively denotes the total matter energy density (pressure), with $\rho_\sigma(p_\sigma)$ denoting the energy density of the scalar field, and a subscript σ denotes the derivative with respect to the scalar field. Because of the NMC, the Newton constant in the Friedmann equations is replaced by $G_N := (8\pi F)^{-1}$ that now varies with time. This has not to be confused with the effective *gravitational constant* that regulates the attraction between two test masses and is measured in laboratory experiments, which is instead given by [42]

$$G_{\text{eff}} = \frac{1}{8\pi F}\left(\frac{2F + 4F_{,\sigma}^2}{2F + 3F_{,\sigma}^2}\right). \quad (3)$$

The deviations from general relativity (GR) can also be parametrized by means of the so-called post-Newtonian (PN) parameters [40], which are given within NMC by the following equations [42]:

$$\gamma_{\text{PN}} = 1 - \frac{F_{,\sigma}^2}{F + 2F_{,\sigma}^2}, \quad (4)$$

---

[1]See Refs. [32,33] for recent proposals that reduce the degree of fine-tuning in EDE models.

[2]See also Ref. [34] for a related mechanism in the framework of an exponentially coupled cubic Galileon model.

[3]Note that the choice of $V \propto F^2$ corresponds to a cosmological constant in the corresponding Einstein frame ($\hat{g}_{\mu\nu} \propto Fg_{\mu\nu}$) in which the canonically rescaled scalar field is universally coupled to the trace of the matter energy-momentum tensor.

$$\beta_{PN} = 1 + \frac{F F_{,\sigma}}{8F + 12F_{,\sigma}^2} \frac{d\gamma_{PN}}{d\sigma}, \qquad (5)$$

where the prediction from GR, i.e., $\gamma_{PN} = \beta_{PN} = 1$, is tightly constrained from the Solar System experiments. Note that $\gamma_{PN} < 1$ in our models.

Before analyzing the background evolution of our model, note that the NMC to the gravity sector induces some conditions that the theory needs to satisfy in order to have a stable FLRW evolution. For the action (1), we find that there are in total 3 physical degrees of freedom associated with the gravity sector (that is, the metric and the σ field) [43]. In order to avoid negative kinetic energy states in the tensor sector, we need

$$F > 0, \qquad (6)$$

and the positivity of the kinetic term in the reduced quadratic action of the scalar field perturbations leads to the second condition

$$F(2F + 3F_{,\sigma}^2) > 0. \qquad (7)$$

For the matter sector, any fluid that satisfies the null energy condition and has real sound speed will be stable. Note that the conditions (6) and (7) also ensure the positivity of the effective gravitational and cosmological Newton constants.

The evolution of relevant background quantities is shown in Fig. 1 for the case of $n = 2$ and $n = 4$ (see caption for the parameters used in the plots). As can be seen from the central panel in Fig. 1, the scalar field is nearly frozen deep in the radiation era, and is driven by the coupling to non-relativistic matter around the radiation-matter equality era $z \sim \mathcal{O}(10^3$–$10^4)$, as evident from the Klein-Gordon equation (2b), decreasing (growing) for $\xi < 0$ ($\xi > 0$).

Since the goal of our paper is to ease the H_0 tension, we also plot the relevant quantities for two other reference models, i.e., the case of a varying number of relativistic degrees of freedom in addition to ΛCDM, and the Rock'n Roll model introduced Ref. [27]. This second model is a representative case of EDE models in Einstein gravity [26–30], where a non-negligible energy density is injected around recombination, leading to a larger value of H_0.

Let us now stress the important differences between the model studied here and the two other reference cases. By considering our model as Einstein gravity [42,43], the resulting effective DE has an equation of state $w_{DE} \equiv p_{DE}/\rho_{DE} \sim 1/3$ during radiation era (see, e.g., Fig. 2 of Ref. [37] and their Eqs. (13) and (14) for the definitions of ρ_{DE} and p_{DE}) and the contribution of the scalar field[4] to the
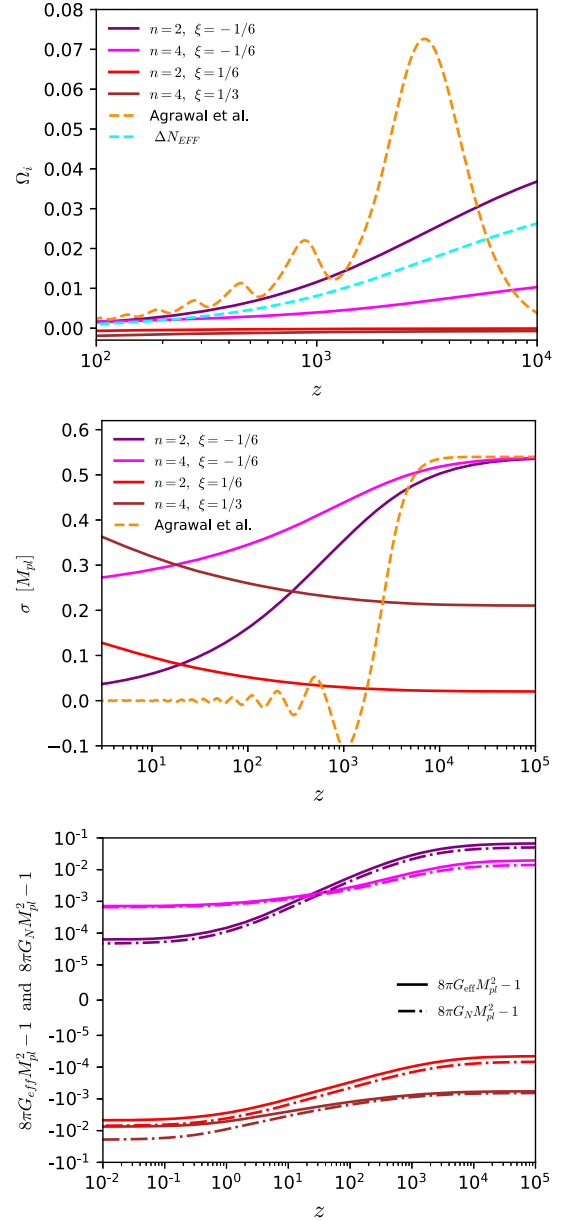

FIG. 1. We plot the evolution of the energy injection $\Omega_i := \rho_i/\rho_c$ (top), the scalar field (center), and the deviation from one of the effective (solid lines) and cosmological (dot-dashed lines) Newton constants (bottom) for the models with $n = 2$, $\xi < 0$ (purple lines), $n = 4$, $\xi < 0$ (magenta lines), $n = 2, \xi > 0$ (red lines), and $n = 4, \xi > 0$ (brown lines), together with the EDE model of Ref. [27] (orange lines) and the ΛCDM $+ N_{eff}$ model (cyan lines). In order to compare the evolution of our model to the aforementioned ones, we set the cosmological parameters to the best fit values in Table 3 of Ref. [27] and set $\xi = -1/6$. In the cases with $\xi > 0$, we change the values of the initial conditions on the scalar field and the coupling ξ as in the plot legends.

---

[4]Note that Ω_σ becomes slightly negative in Fig. 1. This is not a physical problem as Ω_σ only parametrizes the contribution of the scalar field to the total expansion rate $H(z)$ when the Einstein equations are written in the Einstein gravity form; see, e.g., Refs. [42,43].

total expansion rate $H(z)$ thus resembles the one from an extra dark radiation component. This is confirmed by the top panel in Fig. 1, where we plot the energy fraction of the scalar field, parametrized by $\Omega_\sigma = \rho_{DE}/3H^2 F_0$—where
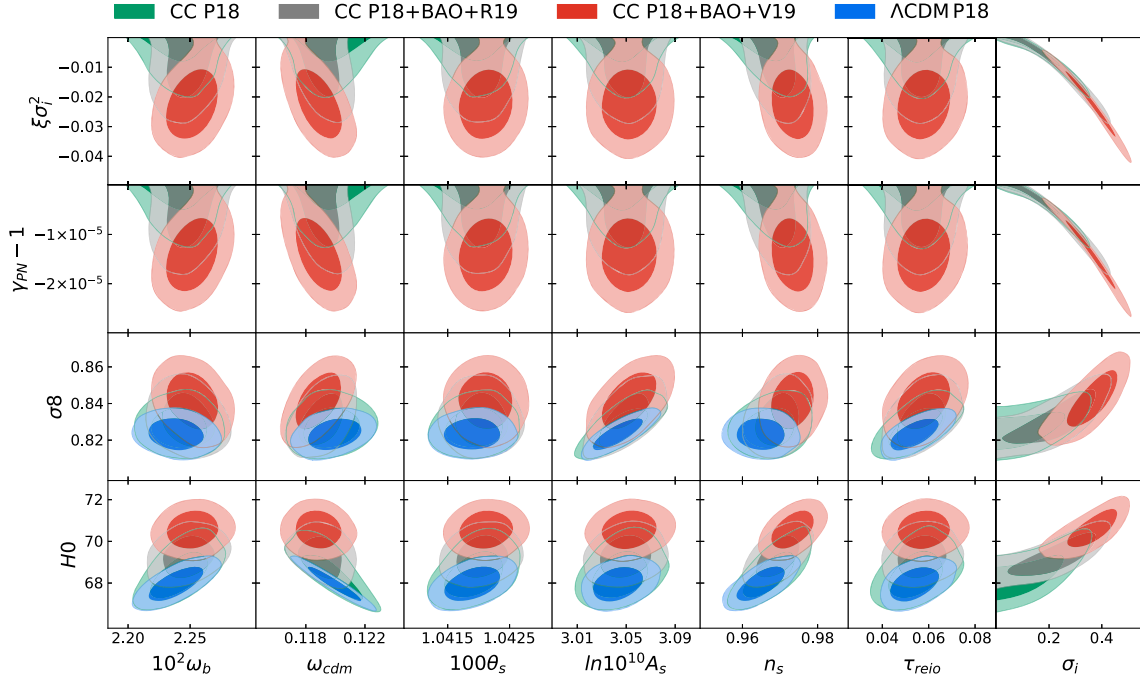
FIG. 2.   Constraints on main and derived parameters of the CC model with $n = 2$ and $\xi = -1/6$ from Planck 2018 data (P18), P18 in combination with BAO and SH0ES measurements, and P18 in combination with BAO and a combined prior which takes into account all the late-time measurements. Parameters on the bottom axis are our sampled MCMC parameters with flat priors, and parameters on the left axis are derived parameters (with H_0 in [km s^{-1} Mpc^{-1}]). Constraints for the ΛCDM model obtained with P18 data are also shown for a comparison. Contours contain 68% and 95% of the probability.

the subscript 0 denotes quantities evaluated at $z = 0$—and compare it to the ΛCDM $+ N_{\mathrm{eff}}$ model. As can be seen, when $\xi < 0$, the scalar field contributes to the total energy density in a way that is very similar to the ΛCDM $+ N_{\mathrm{eff}}$ model. Having started with the same $\xi < 0$ and initial condition $\sigma_i/M_{\mathrm{pl}} < 1$ in both the $n = 2$ and $n = 4$ case, the term multiplying the square bracket in Eq. (2b) is smaller in the latter case and the rolling of the scalar field toward smaller values is less efficient. The equation of state w_{DE} is not $1/3$ anymore in general when the scalar field is subsequently driven by matter.

Our model is therefore different from EDE models recently proposed in the literature (see, e.g., Refs. [26–30]) for which the equation of state is close to -1 at early times. Note also that, in our model, the scalar field moves in a natural way after radiation-matter equality, being driven by nonrelativistic matter, and is not important just around recombination.

In general, a distinct feature of our model is the modification to gravity induced by σ which is plotted in the bottom panel of Fig. 1. For $\xi < 0$, since the scalar field contribution becomes negligible at late times, both G_N and G_{eff} are very close to G today. For this reason, our model is consistent with laboratory and Solar System experiments for a large volume of the parameter space, as we will show in this paper. We do not show the evolution of the PN parameters defined in Eqs. (4) and (5) as they behave similarly.

III. METHODOLOGY AND DATA SETS

We run a Markov-chain Monte Carlo (MCMC) using the publicly available code MontePython-v3[5] [44,45] wrapped either with CLASSig [35], a modified version of the CLASS[6] [46,47] for scalar-tensor theory of gravity, or with a modified version of hiCLASS [48,49] which allows to study consistently oscillating scalar fields. The agreement of CLASSig and hiCLASS for the precision of current and future experiments has been demonstrated in [50]. Mean values and uncertainties on the parameters reported, as well as the contours plotted, have been obtained using GetDist[7] [51]. For all our runs, we set the scalar field in slow roll and use adiabatic initial conditions for the scalar field perturbations [37,52].

We study cosmological models in Eq. (1) with $n = 2, 4$ and free ξ and devote particular attention to the value of $\xi = -1/6$, which is obviously nested in the previous class with $n = 2$. We sample the cosmological parameters $\{\omega_b, \omega_{cdm}, \theta_s, \ln 10^{10} A_s, n_s, \tau_{\mathrm{reio}}, \xi, \sigma_i\}$ fixing $n = 2, 4$ and using Metropolis-Hastings algorithm. We consider flat priors consistent with the stability conditions in Sec. II on the extra parameters we consider $\xi \in [-0.9, 0.9]$ and $\sigma_i/M_{\mathrm{pl}} \in [0, 0.9]$, for $n = 2$ case with free

ξ and $\sigma_i/M_{\rm pl} \in [0, 0.9]$ in the CC case. For the case with $n = 4$, we change our prior to $\xi \in [-0.9, 0.2]$ as larger positive values for the coupling ξ lead to a deviation of order 10^{-1} from GR as can be seen from Fig. 1. As in [36], we take into account the different value of the effective gravitational constant in the modified BBN condition for the helium, and the baryon density tabulated in the public code PArthENoPE [53]. We consider the chains to be converged using the Gelman-Rubin criterion $R - 1 < 0.01$.

We constrain the cosmological parameters using several combination of data sets. We use the CMB measurements from the Planck 2018 release (hereafter P18) on temperature, polarization, and weak lensing CMB angular power spectra [54,55]. We use the following likelihood combination, the so-called Planck baseline: on high multipoles, $\ell \geq 30$, we use the Plik likelihood, on the lower multipoles we use the Commander likelihood for temperature and SimAll for the E-mode polarization [54], for the lensing likelihood we the conservative multipoles range, i.e., $8 \leq \ell \leq 400$ [55].

BAO measurements from galaxy redshift surveys are used as primary astrophysical data set to constrain these class of theories providing a complementary late-time information to the CMB anisotropies. We use the Baryon Oscillation Spectroscopic Survey DR12 [56] "consensus" in three redshift slices with effective redshifts $z_{\rm eff} = 0.38, 0.51, 0.61$ [57–59] in combination with measurements from 6dF [60] at $z_{\rm eff} = 0.106$ and the one from SDSS DR7 [61] at $z_{\rm eff} = 0.15$. We consider a Gaussian likelihood based on the latest determination of H_0 from SH0ES, i.e., $H_0 = 74.03 \pm 1.42~{\rm km\,s^{-1}\,Mpc^{-1}}$ [3], which we will denote as R19 in the following. We also consider a tighter Gaussian likelihood, i.e., $H_0 = 73.3 \pm 0.8~{\rm km\,s^{-1}\,Mpc^{-1}}$ [1], obtained from a combination of H_0 measurements from SH0ES [3], MIRAS [62], CCHP [7], H0LiCOW [12], MCP [63], and SBF which we will denote as V19 in the following. We should warn the reader that the V19 value is obtained by neglecting covariances between the aforementioned observations, as stressed in Ref. [1]. Nevertheless, V19 can give an idea of how our model can respond to a possible future worsening of the H_0 tension.

Note that our analysis differs from [37] not only in the updated data, but also in theoretical priors: in this paper, we consider flat priors on (ξ, σ_i), whereas in [37], flat priors were assumed on $(\xi, M_{\rm pl})$, with $\xi > 0$ and $\xi < 0$ considered separately, and $M_{\rm pl}$ was also allowed to vary, with a boundary condition on σ_0 (the value of the scalar field today) to fix consistency between $G_{\rm eff}$ and G. We have however verified that these different priors have a very small effect on the resulting posterior distributions of the parameters, at least for $\xi = -1/6$.

IV. RESULTS

The results of our cosmological analysis for the CC ($n = 2$ with free ξ) model are summarized in Fig. 2 (Fig. 3),

where we plot the reconstructed two-dimensional posterior distributions of main and derived parameters, and in Table I (Table II), where we report the reconstructed mean values and the 68% and 95% CL. We also report our results for the $n = 4$ case in Table III.

We find similar values for H_0 in all the models, but larger than in ΛCDM. We find $H_0 = 68.47^{+0.58}_{-0.86}$ ($H_0 = 68.40^{+0.59}_{-0.80}$) ${\rm km\,s^{-1}\,Mpc^{-1}}$ at 68% CL for CC (for free ξ) with P18 data only. As in other similar models, we find larger values for n_s, ω_c, σ_8 and smaller values for ω_b compared to the baseline ΛCDM model. When BAO and SH0ES data are combined, i.e., P18 + BAO + R19, we obtain $H_0 = 69.29^{+0.59}_{-0.72}$ ($H_0 = 69.10^{+0.49}_{-0.66}$) ${\rm km\,s^{-1}\,Mpc^{-1}}$ for CC (for free ξ). Higher values for H_0 can be obtained by substituting the combination of measurements V19 to R19, as can be seen from Tables I and II. Note that similar results are also obtained in the $n = 4$ case, for which we find a slightly smaller value of $H_0 = 68.05 \pm 0.56$ ($H_0 = 69.09^{+0.52}_{-0.69}$) ${\rm km\,s^{-1}\,Mpc^{-1}}$ with P18 (P18 + BAO + R19) data. For this reason, we focus our discussion on the $n = 2$ case in the following, commenting only when results for $n = 4$ substantially differ.

In Tables–III, we also report the difference in the best fit of the model with respect to ΛCDM, i.e., $\Delta\chi^2 = \chi^2 - \chi^2(\Lambda{\rm CDM})$, where negative values indicate an improvement in the fit of the given model with respect to the ΛCDM for the same data set.[8] Although our models provide a similar or slightly worst fit to P18 data compared to ΛCDM, we find $\Delta\chi^2 \sim -5$ (-6.8) for CC (free ξ) when BAO + R19 are combined. Higher values of $\Delta\chi^2$ are obviously obtained by substituting V19 to R19. We also compute values of the Aikike (Bayes) information criteria $\Delta{\rm AIC}$ ($\Delta{\rm BIC}$) defined as $\Delta{\rm AIC} = \Delta\chi^2 + 2\Delta p$ ($\Delta{\rm BIC} = \Delta\chi^2 + \Delta p \ln N$), where Δp is the number of extra parameters with respect to ΛCDM model and N is the number of data points considered in our MCMC analysis[9] [64]. According to both criteria, all our models are penalized compared to ΛCDM for P18 data only due to the addition of parameters. Only for AIC we find that our model with $n = 2$ is (strongly) favored for (CC) free ξ compared to ΛCDM when BAO and R19 are combined. Substituting V19 to R19 makes the statistical preference of our model stronger in general.

---

[8]Note that the ΛCDM reference cosmology in our case has massless neutrinos, differently from the assumption adopted by the Planck Collaboration of one massive neutrino with $m_\nu = 0.06$ eV consistent with a normal hierarchy with minimum mass allowed by particle physics. The differences with respect to the baseline Planck results in the estimate of the cosmological parameters due the choice $N_{\rm eff} = 3.046$ and $m_\nu = 0$ is small, except for a shift toward higher values for H_0, as $H_0 = 67.98 \pm 0.54$ ($H_0 = 68.60 \pm 0.43$) ${\rm km\,s^{-1}\,Mpc^{-1}}$ for P18 (P18 + BAO + R19).

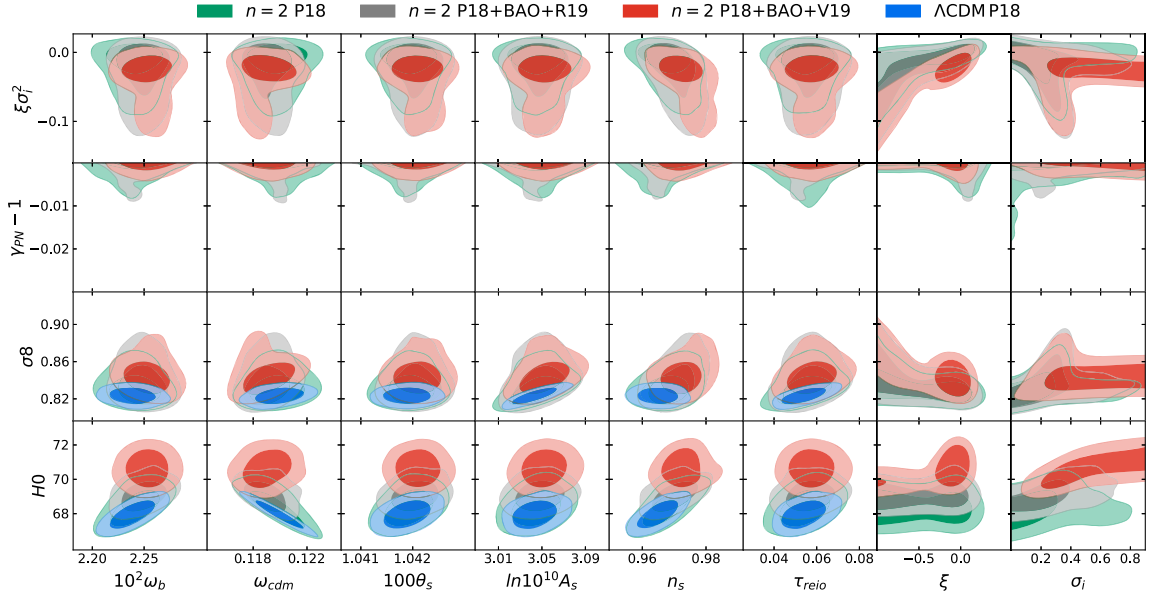[9]We consider 2352 points for P18, 8 for BAO and 1 (6) for R19 (V19).

FIG. 3.   Constraints on main and derived parameters of the model with $n = 2$ and ξ as a main parameter from Planck 2018 data (P18), P18 in combination with BAO and SH0ES measurements, and P18 in combination with BAO and a combined prior which takes into account all the late-time measurements. Parameters on the bottom axis are our sampled MCMC parameters with flat priors, and parameters on the left axis are derived parameters (with H_0 in [km s^{-1} Mpc^{-1}]). Constraints for the ΛCDM model obtained with P18 data are also shown for a comparison. Contours contain 68% and 95% of the probability.

Constraints on modified gravity parameters: The constraints on the modified gravity parameter are very different in the CC and $n = 2$ case, which are a one- and two-parameter extension of the ΛCDM model. Although the mean values are very similar, constraints are very much looser in the latter case. This is because, when ξ is large and negative, the decreasing of the scalar field is very efficient and thus its effect redshifts away even before matter-radiation equality, leaving smaller imprints on the CMB. Note that positive values of ξ, for which the scalar field increases after matter-radiation equality contributing to the late-time background evolution, seem disfavored by the data for our priors. In particular for P18, we find an upper bound $\xi < 0.052$ ($\xi < 0.02$) at the 2σ level for $n = 2$ ($n = 4$). The upper bound is even more stringent when we add to the analysis BAO + R19 data for which we find $\xi < 0.047$ ($\xi < -0.026$) at the 2σ level for $n = 2$ ($n = 4$).

Comparison with BBN constraints: With our priors, the departure of $\sqrt{F}$ from $M_{\rm pl}$ can also be constrained by BBN [65–67]. Since the scalar field is frozen at very early times, the BBN constraints reported in [65,66] would imply $\xi\sigma_i^n = 0.01^{+0.20}_{-0.16}$ at 68% CL, which are consistent, but less stringent, than the constraints reported in Tables I–III, as already mentioned in previous works on scalar tensor [36]. We find $-0.014^{+0.026}_{-0.052}$ (>-0.0150) for the $n = 2$ (CC[10]) and $-0.0010^{+0.0029}_{-0.0076}$ for the $n = 4$ case at 95% CL using P18

---

[10]Note that, in the CC case, $\xi\sigma_i^2 < 0$ by construction.

data only. When adding BAO+R19, we obtain a higher $\xi\sigma_i^n$ and the constraints change to $-0.025^{+0.037}_{-0.070}$ (>-0.0234) for the $n = 2$ (CC) and $-0.013^{+0.021}_{-0.038}$ for the $n = 4$ case at 95% CL. Note that $\xi\sigma_i^n$ is more constrained in the CC case compared to $n = 2$ and $n = 4$, as the coupling is fixed to $\xi = -1/6$.

Comparison with PN: The derived cosmological PN parameters are well consistent with GR and their uncertainties are comparable with bounds from the Solar System experiments [39,40]. Again, because of the large errors on ξ, the bounds in the $n = 2$ model are somewhat looser than in the CC model. Therefore, the CC ($n = 2$) model potentially offers a simple one (two) modified gravity parameter extension to the baseline ΛCDM that naturally eases the H_0 tension and can be consistent at 2σ with the Solar System constraints on deviation from GR. We have checked that the inclusion of the Solar System constraints in our analysis by means of a Gaussian prior based on the Cassini constraint $\gamma_{\rm PN} - 1 = 2.1 \pm 2.3 \times 10^{-5}$ [39] has a very small impact on our constraints on the six standard cosmological parameters.

For the representative example of $n = 2$ with free ξ, the constraint on H_0 obtained from P18 + BAO + R19 changes to $H_0 = 69.00^{+0.47}_{-0.57}$ km s^{-1}Mpc^{-1}. The constraints on the modified gravity parameters instead change substantially. Thanks to the constraining power of the prior we find $\sigma_i = 0.19^{+0.13}_{-0.08} M_{\rm pl}$ at 68% CL and $\gamma_{\rm PN} - 1 > -2.2 \times 10^{-6}$ and a bound on $\xi < -0.15$ at 95% CL. Although ξ remains unconstrained, we note that the upper limit is

TABLE I. Constraints on main and derived parameters considering P18, P18 in combination with BAO and SH0ES measurements, and P18 in combination with BAO and a combined prior which takes into account all the late-time measurements for the CC model $n = 2$ and $\xi = -1/6$. We report mean values and the 68% CL, except for the modified gravity derived parameters in the third block, for which we report the 95% CL.

CC	P18	P18 + BAO + R19	P18 + BAO + V19
$10^2 \omega_b$	2.242 ± 0.015	2.248 ± 0.014	2.252 ± 0.013
ω_c	0.1197 ± 0.0012	$0.119\,10 \pm 0.000\,99$	0.1188 ± 0.0010
$100 * \theta_s$	$1.041\,94 \pm 0.000\,30$	$1.042\,05 \pm 0.000\,28$	$1.042 \pm 0.000\,28$
τ_{reio}	0.0547 ± 0.0077	0.0570 ± 0.0071	$0.058\,03 \pm 0.0075$
$\ln(10^{10} A_s)$	3.046 ± 0.015	3.049 ± 0.014	3.053 ± 0.015
n_s	0.9675 ± 0.0046	0.9695 ± 0.0038	0.9734 ± 0.0037
σ_i [M_{pl}]	$0.1312^{+0.039}_{-0.13}$	$0.224^{+0.13}_{-0.081}$	$0.3585^{+0.078}_{-0.047}$
H_0 [km s^{-1} Mpc^{-1}]	$68.47^{+0.58}_{-0.86}$	$69.29^{+0.59}_{-0.72}$	70.56 ± 0.6
σ_8	$0.8272^{+0.0063}_{-0.0081}$	$0.8313^{+0.0079}_{-0.011}$	0.841 ± 0.010
r_s [Mpc]	$146.97^{+0.33}_{-0.29}$	$146.83^{+0.48}_{-0.34}$	146.4 ± 0.45
$\xi \sigma_i^2$ [M_{pl}^2]	> -0.0150	> -0.0234	$-0.022^{+0.016}_{-0.015}$
σ_0 [M_{pl}]	$0.004\,017^{+0.0012}_{-0.004}$	$0.006\,841^{+0.004}_{-0.0025}$	$0.011\,02^{+0.0024}_{-0.0015}$
$\gamma_{\mathrm{PN}} - 1$	$> -0.95 \times 10^{-5}$	$> -1.5 \times 10^{-5}$	$(-1.4^{+1.0}_{-0.9}) \times 10^{-5}$
$\beta_{\mathrm{PN}} - 1$	$(0.23^{+0.61}_{-0.34}) \times 10^{-6}$	$(0.53^{+0.75}_{-0.61}) \times 10^{-6}$	$(1.16^{+0.78}_{-0.84}) \times 10^{-6}$
$\Delta \chi^2$	$+0.42$	-5.0	-13.64

tighter than the one obtained without the prior information on γ_{PN}. Negative values of ξ are more favored as they lead to a more efficient rolling of the scalar field toward smaller values and therefore a smaller $\gamma_{\mathrm{PN}} - 1$.

Robustness and caveats of the inclusion of SNe data: So far, we did not use the SNe Ia luminosity distance because the time evolution of gravitational constant changes the peak luminosity of SNe and this needs to be properly

TABLE II. Constraints on main and derived parameters considering P18, P18 in combination with BAO and SH0ES measurements, and P18 in combination with BAO and a combined prior which takes into account all the late-time measurements for $n = 2$. We report mean values and the 68% CL, except for the modified gravity derived parameters in the third block, for which we report the 95% CL.

$n = 2$	P18	P18 + BAO + R19	P18 + BAO + V19
$10^2 \omega_b$	2.241 ± 0.015	2.249 ± 0.014	2.253 ± 0.014
ω_c	0.1198 ± 0.0012	$0.119\,03^{+0.000\,95}_{-0.0011}$	0.1190 ± 0.0012
$100 * \theta_s$	$1.041\,93 \pm 0.000\,30$	$1.042\,05 \pm 0.000\,31$	$1.042\,10 \pm 0.000\,29$
τ_{reio}	0.0544 ± 0.0076	0.0564 ± 0.0076	0.0578 ± 0.0072
$\ln(10^{10} A_s)$	3.045 ± 0.0014	3.048 ± 0.015	3.052 ± 0.014
n_s	0.9673 ± 0.0046	0.9699 ± 0.0046	0.9724 ± 0.0041
σ_i [M_{pl}]	< 0.224	$0.260^{+0.088}_{-0.19}$	> 0.46
ξ	< 0.052 (95% CL)	< 0.047 (95% CL)	< -0.0283 (95% CL)
H_0 [km s^{-1} Mpc^{-1}]	$68.40^{+0.59}_{-0.80}$	$69.10^{+0.49}_{-0.66}$	70.64 ± 0.71
σ_8	$0.8456^{+0.013}_{-0.018}$	$0.8370^{+0.0072}_{-0.020}$	$0.8450^{+0.0088}_{-0.014}$
r_s [Mpc]	147.01 ± 0.36	$146.95^{+0.48}_{-0.30}$	$146.08^{+0.77}_{-0.89}$
$\xi \sigma_i^2$ [M_{pl}^2]	$-0.014^{+0.026}_{-0.052}$	$-0.025^{+0.037}_{-0.070}$	$-0.030^{+0.030}_{-0.074}$
σ_0 [M_{pl}]	$0.1046^{+0.40}_{-0.18}$	$0.09^{+0.46}_{-0.19}$	$0.20^{+0.33}_{-0.26}$
$\gamma_{\mathrm{PN}} - 1$	$> -1.73 \times 10^{-3}$	$> -1.56 \times 10^{-3}$	$> -1.26 \times 10^{-3}$
$\beta_{\mathrm{PN}} - 1$	$-(3.0^{+1.8}_{-1.6}) \times 10^{-5}$	$-(3.0^{+1.7}_{-1.4}) \times 10^{-5}$	$-(1.5^{+2.9}_{-2.5}) \times 10^{-5}$
$\Delta \chi^2$	$+0.52$	-6.8	-18.44

TABLE III. Constraints on main and derived parameters considering P18, P18 in combination with BAO and SH0ES measurements, and P18 in combination with BAO and a combined prior which takes into account all the late-time measurements for $n = 4$. We report mean values and the 68% CL, except for the modified gravity derived parameters in the third block, for which we report the 95% CL.

$n = 4$	P18	P18 + BAO + R19	P18 + BAO + V19
$10^2 \omega_b$	2.240 ± 0.015	2.250 ± 0.013	2.258 ± 0.013
ω_c	0.1198 ± 0.0012	0.11892 ± 0.00093	0.11830 ± 0.00097
$100 * \theta_s$	1.04190 ± 0.00028	1.04205 ± 0.00028	1.04217 ± 0.00028
τ_{reio}	0.0545 ± 0.0074	0.0564 ± 0.0076	$0.0596^{+0.0070}_{-0.0078}$
$\ln(10^{10} A_s)$	3.045 ± 0.014	3.049 ± 0.015	3.055 ± 0.015
n_s	0.9662 ± 0.0043	$0.9706^{+0.0037}_{-0.0042}$	$0.9757^{+0.0039}_{-0.0044}$
σ_i [M$_{\mathrm{pl}}$]	<0.257	$0.37^{+0.20}_{-0.17}$	$0.55^{+0.13}_{-0.11}$
ξ	<0.02 (95% CL)	<-0.026 (95% CL)	<-0.031 (95% CL)
H_0 [km s^{-1} Mpc^{-1}]	68.05 ± 0.56	$69.09^{+0.52}_{-0.69}$	70.23 ± 0.54
σ_8	0.8247 ± 0.0061	$0.8370^{+0.0072}_{-0.020}$	$0.845^{+0.010}_{-0.018}$
r_s [Mpc]	147.06 ± 0.28	$146.96^{+0.39}_{-0.33}$	$146.69^{+0.38}_{-0.43}$
$\xi \sigma_i^4$ [M_{pl}^4]	$-0.0010^{+0.0029}_{-0.0076}$	$-0.013^{+0.021}_{-0.038}$	$-0.035^{+0.038}_{-0.057}$
σ_0 [M$_{\mathrm{pl}}$]	$0.18^{+0.39}_{-0.22}$	$0.18^{+0.25}_{-0.17}$	$0.20^{+0.21}_{-0.13}$
$\gamma_{\mathrm{PN}} - 1$	$>-1.72 \times 10^{-4}$	$>-1.65 \times 10^{-4}$	$>-2.34 \times 10^{-4}$
$\beta_{\mathrm{PN}} - 1$	$(-0.8^{+11.0}_{-9.4}) \times 10^{-6}$	$(0.4^{+6.1}_{-3.8}) \times 10^{-6}$	$(2.5^{+7.4}_{-6.6}) \times 10^{-6}$
$\Delta\chi^2$	-0.58	-1.14	-9.42

accounted in the analysis [68–71]. However, for the best-fit value obtained from P18 + BAO + R19 with the priors on γ_{PN}, the relative change of G_{eff} from G today is at most 10^{-5} in the relevant range of redshifts for SNe Ia. Under the assumption that we can ignore the effect of time evolution of G_{eff} on the magnitude-redshift relation of SNe Ia, we use the Pantheon sample of SNe to check the robustness of our constraint on H_0 [72]. We obtain $H_0 = 69.28^{+0.58}_{-0.74}$ ($H_0 = 68.98^{+0.46}_{-0.54}$) km s^{-1} Mpc^{-1} for CC (for free ξ) using P18 + BAO + R19+Pantheon with the prior on γ_{PN}. This shows that the inclusion of SNe Ia data does not change the constraint on H_0. Note also that the modification of the gravitational constant can also change the low-redshift distance-ladder measurements of the Hubble constant [73,74]. However, again due to the smallness of the relative change of G_{eff} from G today, this effect can be ignored safely in our models.

Comparison with other EDE models: Models based on a sharp energy injection around the time of matter-radiation equality lead to a value of H_0 which can be higher than the ones we found within our model for any choice of n and ξ, although this is model dependent (see, e.g., Refs. [26–30]). However, the radiationlike behavior of the scalar field in theories described by the action (1) is completely generic and, provided that the coupling ξ is negative, the scalar field contribution quickly becomes negligible thanks to the coupling to nonrelativistic matter and modifies essentially only the early time dynamics. For this reason, a higher H_0 than in ΛCDM is a natural outcome of the NMC for a large

portion of the parameter space compared to EDE models, which have more extra parameters to tune.

Addition of N_{eff}: As already mentioned in the Introduction, the archetypal way to reduce the sound horizon at baryon drag is to allow the number of relativistic species N_{eff} to vary [16,17]. By varying N_{eff}, we find for P18 + BAO + R19 $\Delta\chi^2 \sim -2.8$ with $H_0 = 70.01 \pm 0.89$ km s^{-1} Mpc^{-1} and $N_{\mathrm{eff}} = 3.30 \pm 0.14$. Despite the higher mean value for H_0, the improvement in the fit is smaller than what we obtain for CC case, and even smaller for NMC with $n = 2$. We then investigate to which extent the addition of extra relativistic species (N_{eff}) to our model with $n = 2$ can further ease the tension.

We allow N_{eff} to vary with a flat prior $N_{\mathrm{eff}} \in [0, 6]$ and we restrict to the combination of P18, BAO, and V19. The results of our analysis are shown in Fig. 4, where we plot for the CC and $n = 2$ case the two-dimensional posterior distributions of the main parameters σ_i and N_{eff} and the derived H_0, γ_{PN}, and $\xi \sigma_i^2$.

To provide the reader with a comparison, we also plot the constraints on the ΛCDM + N_{eff} model for the same data set. As in the case where N_{eff} is fixed, constraints on the other cosmological parameters are nearly the same in both the models. Again, we find very similar results, i.e., $N_{\mathrm{eff}} = 3.43^{+0.16}_{-0.13}$, $H_0 = 71.45 \pm 0.68$ km s^{-1} Mpc^{-1} in the CC model and $N_{\mathrm{eff}} = 3.44^{+0.15}_{-0.12}$, $H_0 = 71.44 \pm 0.67$ km s^{-1} Mpc^{-1} in the $n = 2$ model at 68% CL. It is interesting to note that the value we find $\Delta N_{\mathrm{eff}} \sim 0.39$ is similar to the case of an additional thermalized massless
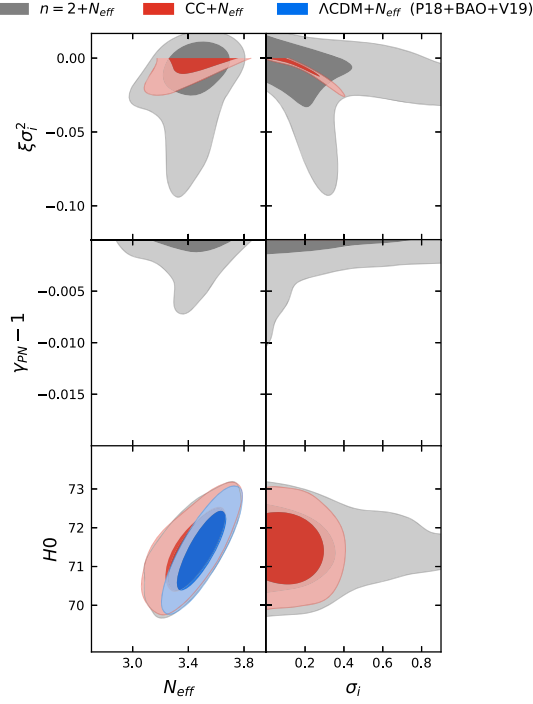
FIG. 4. Constraints on some of the main and derived parameters of the CC and $n = 2$ model with the addition of N_{eff} from P18 in combination with BAO and a combined prior which takes into account all the late-time measurements. Parameters on the bottom axis are our sampled MCMC parameters with flat priors, and parameters on the left axis are derived parameters (with H_0 in [km s^{-1} Mpc^{-1}]). Contours contain 68% and 95% of the probability.

boson which decouples at a temperature $T > 100$ MeV [75]. We note that the relevant parameter that regulates the scalar field modification to $H(z)$, that is $\xi\sigma_i^2$, is now much smaller than in the correspondent case with N_{eff} fixed (see Tables I and II), that is $\xi\sigma_i^2 > -0.0193$ in the CC model and $\xi\sigma_i^2 = -0.012^{+0.018}_{-0.003}$ in the $n = 2$ model: this means that the higher value of H_0 is now driven by a combination of a higher N_{eff} with the nonminimally coupled scalar field σ. In fact, in the case of the $\Lambda\text{CDM} + N_{\text{eff}}$ model, we find a larger $N_{\text{eff}} = 3.50 \pm 0.12$ at 68% CL consistently with the scalar field effectively contributing as an extra dark radiation component in the CC and $n = 2$ case.

V. DISCUSSION AND CONCLUSIONS

In this paper, we have studied the addition of a cosmological massless scalar field σ to ΛCDM with a coupling to the Ricci scalar of the form $F(\sigma) = M_{\text{pl}}^2[1 + \xi(\sigma/M_{\text{pl}})^n]$, in the case of $n = 2, 4$. This class of models has one (as for CC) or two extra parameters with respect to ΛCDM. The scalar field σ is frozen deep in the radiation era, essentially contributing to the expansion history of the Universe as an effective relativistic degree of freedom, and the coupling to nonrelativistic matter acts as a driving force for the scalar

field around radiation-matter equality [35–37]. The basic assumption of a cosmological constant Λ minimizes the deviations from ΛCDM at late time which are present in scalar-tensor theories and allows to focus on the early time dynamics.

We have used the most recent Planck, BAO, and SH0ES data to perform a MCMC analysis and constrain the parameters of our model. We find that Planck 18 (+BAO+R19) constrains the expansion rate of the Universe from $H_0 = 68.40^{+0.59}_{-0.80}$ ($H_0 = 69.10^{+0.49}_{-0.66}$) km s^{-1} Mpc^{-1} for $n = 2$. Similar results for the cosmological parameters can also be obtained in the CC case.

Compared to other attempts to alleviate the H_0 tension such as EDE models, we obtain a lower expansion rate. However, we stress that EDE models require two or three extra parameters with respect to ΛCDM, which have to be fine-tuned to inject the precise amount of energy to the cosmic fluid in a very narrow range of redshift. The models considered here have only one or two extra parameters and can be easily embedded in a consistent theoretical framework of scalar-tensor theories of gravity.

We find that our constraints on $\xi\sigma^n$, the deviation from GR, are consistent with those obtained from BBN [65,66] and the constraints on the PN parameters from the Solar System measurements [39,40]. Higher values for H_0 can be obtained by further allowing N_{eff} to vary or by using the tighter prior V19 on H_0 rather than R19. In the former case, we find tighter constraints on $\xi\sigma_i^n$ that regulates the scalar field contribution to the expansion history during the radiation era and the larger value of H_0 is driven by a cooperation with the extra relativistic species described by N_{eff}.

Note added.—While this project was near to completion, a related paper [76], also studying how a massless nonminimally coupled scalar field with $n = 2$ with a flat potential could ease the tension, appeared. Where a comparison is possible, we find consistency in the estimate of cosmological parameters, but our findings for $\Delta\chi^2$ are at odds with [76]. Not only NMC with $n = 2$ leads to a larger improvement in the fit than the addition of N_{eff} for P18 + BAO + R19, but also the CC does.

---

[1] L. Verde, T. Treu, and A. G. Riess, Tensions between the Early and the Late Universe, Nat. Astron. **3**, 891 (2019).

[2] N. Aghanim *et al.* (Planck Collaboration), Planck 2018 results. VI. Cosmological parameters, arXiv:1807.06209.

[3] A. G. Riess, S. Casertano, W. Yuan, L. M. Macri, and D. Scolnic, Large magellanic cloud cepheid standards provide a 1% foundation for the determination of the Hubble constant and stronger evidence for physics beyond \ΛCDM, Astrophys. J. **876**, 85 (2019).

[4] A. G. Riess *et al.*, Milky Way cepheid standards for measuring cosmic distances and application to Gaia DR2: Implications for the Hubble constant, Astrophys. J. **861**, 126 (2018).

[5] P. Lemos, E. Lee, G. Efstathiou, and S. Gratton, Model independent $H(z)$ reconstruction using the cosmic inverse distance ladder, Mon. Not. R. Astron. Soc. **483**, 4803 (2019).

[6] G. Efstathiou, H0 revisited, Mon. Not. R. Astron. Soc. **440**, 1138 (2014).

[7] W. L. Freedman *et al.*, The carnegie-chicago Hubble program. VIII. An independent determination of the Hubble constant based on the tip of the red giant branch, Astrophys. J. **882**, 34 (2019).

[8] W. L. Freedman, B. F. Madore, T. Hoyt, I. Sung Jang, R. Beaton, M. Gyoon Lee, A. Monson, J. Neeley, and J. Rich, Calibration of the Tip of the Red Giant Branch (TRGB), Astrophys. J. **891**, 57 (2020).

[9] W. Yuan, A. G. Riess, L. M. Macri, S. Casertano, and D. Scolnic, Consistent calibration of the tip of the red giant branch in the large magellanic cloud on the Hubble space telescope photometric system and a re-determination of the Hubble constant, Astrophys. J. **886**, 61 (2019).

[10] M. Rigault *et al.*, Confirmation of a star formation bias in type Ia supernova distances and its effect on measurement of the Hubble constant, Astrophys. J. **802**, 20 (2015).

[11] M. Rigault *et al.* (Nearby Supernova Factory Collaboration), Strong Dependence of Type Ia Supernova Standardization on the Local Specific Star Formation Rate, arXiv:1806.03849.

[12] K. C. Wong *et al.*, H0LiCOW XIII. A 2.4% measurement of H_0 from lensed quasars: 5.3σ tension between early and late-Universe probes, Mon. Not. R. Astron. Soc. (2020) https://doi.org/10.1093/mnras/stz3094.

[13] J. L. Bernal, L. Verde, and A. G. Riess, The trouble with H_0, J. Cosmol. Astropart. Phys. 10 (2016) 019.

[14] K. Aylor, M. Joy, L. Knox, M. Millea, S. Raghunathan, and W. L. K. Wu, Sounds discordant: classical distance ladder & ΛCDM -based determinations of the cosmological sound horizon, Astrophys. J. **874**, 4 (2019).

[15] L. Knox and M. Millea, Hubble constant hunter's guide, Phys. Rev. D **101**, 043533 (2020).

[16] A. G. Riess, L. Macri, S. Casertano, H. Lampeitl, H. C. Ferguson, A. V. Filippenko, S. W. Jha, W. Li, and R. Chornock, A 3% solution: determination of the Hubble constant with the Hubble space telescope and wide field camera 3, Astrophys. J. **730**, 119 (2011); **732**, 129(E) (2011).

[17] M. Wyman, D. H. Rudd, R. A. Vanderveld, and W. Hu, Neutrinos Help Reconcile Planck Measurements with the Local Universe, Phys. Rev. Lett. **112**, 051302 (2014).

[18] F. Y. Cyr-Racine and K. Sigurdson, Limits on neutrino-neutrino scattering in the early Universe, Phys. Rev. D **90**, 123533 (2014).

[19] L. Lancaster, F. Y. Cyr-Racine, L. Knox, and Z. Pan, A tale of two modes: Neutrino free-streaming in the early universe, J. Cosmol. Astropart. Phys. 07 (2017) 033.

[20] M. A. Buen-Abad, M. Schmaltz, J. Lesgourgues, and T. Brinckmann, Interacting dark sector and precision cosmology, J. Cosmol. Astropart. Phys. 01 (2018) 008.

[21] E. Di Valentino, C. Behm, E. Hivon, and F. R. Bouchet, Reducing the H_0 and σ_8 tensions with Dark Matter-neutrino interactions, Phys. Rev. D **97**, 043513 (2018).

[22] F. D'Eramo, R. Z. Ferreira, A. Notari, and J. L. Bernal, Hot Axions and the H_0 tension, J. Cosmol. Astropart. Phys. 11 (2018) 014.

[23] V. Poulin, K. K. Boddy, S. Bird, and M. Kamionkowski, Implications of an extended dark energy cosmology with massive neutrinos for cosmological tensions, Phys. Rev. D **97**, 123504 (2018).

[24] C. D. Kreisch, F. Y. Cyr-Racine, and O. Dor, The neutrino puzzle: anomalies, interactions, and cosmological tensions, Phys. Rev. D **101**, 123505 (2020).

[25] N. Blinov, K. J. Kelly, G. Z. Krnjaic, and S. D. McDermott, Constraining the Self-Interacting Neutrino Interpretation of the Hubble Tension, Phys. Rev. Lett. **123**, 191102 (2019).

[26] V. Poulin, T. L. Smith, T. Karwal, and M. Kamionkowski, Early Dark Energy Can Resolve The Hubble Tension, Phys. Rev. Lett. **122**, 221301 (2019).

[27] P. Agrawal, F. Y. Cyr-Racine, D. Pinner, and L. Randall, Rock 'n' Roll Solutions to the Hubble Tension, arXiv:1904.01016.

[28] S. Alexander and E. McDonough, Axion-Dilaton destabilization and the Hubble tension, Phys. Lett. B **797**, 134830 (2019).

[29] M. X. Lin, G. Benevento, W. Hu, and M. Raveri, Acoustic dark energy: Potential conversion of the Hubble tension, Phys. Rev. D **100,** 063542 (2019).

[30] T. L. Smith, V. Poulin, and M. A. Amin, Oscillating scalar fields and the Hubble tension: a resolution with novel signatures, Phys. Rev. D **101,** 063523 (2020).

[31] M. Braglia, W. T. Emond, F. Finelli, A. E. Gumrukcuoglu, and K. Koyama, Unified framework for Early Dark Energy from α-attractors, arXiv:2005.14053.

[32] K. V. Berghaus and T. Karwal, Thermal friction as a solution to the Hubble tension, Phys. Rev. D **101,** 083537 (2020).

[33] J. Sakstein and M. Trodden, Early Dark Energy From Massive Neutrinos - A Natural Resolution of the Hubble Tension, Phys. Rev. Lett. **124,** 161301 (2020).

[34] M. Zumalacarregui, Phys. Rev. D **102,** 023523 (2020).

[35] C. Umilt, M. Ballardini, F. Finelli, and D. Paoletti, CMB and BAO constraints for an induced gravity dark energy model with a quartic potential, J. Cosmol. Astropart. Phys. 08 (2015) 017.

[36] M. Ballardini, F. Finelli, C. Umilt, and D. Paoletti, Cosmological constraints on induced gravity dark energy models, J. Cosmol. Astropart. Phys. 05 (2016) 067.

[37] M. Rossi, M. Ballardini, M. Braglia, F. Finelli, D. Paoletti, A. A. Starobinsky, and C. Umilt, Cosmological constraints on post-Newtonian parameters in effectively massless scalar-tensor theories of gravity, Phys. Rev. D **100,** 103524 (2019).

[38] J. Sol Peracaula, A. Gomez-Valent, J. de Cruz Prez, and C. Moreno-Pulido, Brans–Dicke gravity with a cosmological constant smoothes out ΛCDM tensions, Astrophys. J. Lett. **886,** L6 (2019).

[39] B. Bertotti, L. Iess, and P. Tortora, A test of general relativity using radio links with the Cassini spacecraft, Nature (London) **425,** 374 (2003).

[40] C. M. Will, The confrontation between general relativity and experiment, Living Rev. Relativity **17,** 4 (2014).

[41] M. Ballardini, M. Braglia, F. Finelli, D. Paoletti, A. A. Starobinsky, and C. Umilt, Scalar-tensor theories of gravity, neutrino physics, and the H_0 tension, arXiv:2004.14349.

[42] B. Boisseau, G. Esposito-Farese, D. Polarski, and A. A. Starobinsky, Reconstruction of a Scalar Tensor Theory of Gravity in an Accelerating Universe, Phys. Rev. Lett. **85,** 2236 (2000).

[43] R. Gannouji, D. Polarski, A. Ranquet, and A. A. Starobinsky, Scalar-tensor models of normal and phantom dark energy, J. Cosmol. Astropart. Phys. 09 (2006) 016.

[44] B. Audren, J. Lesgourgues, K. Benabed, and S. Prunet, Conservative Constraints on Early Cosmology: an illustration of the Monte Python cosmological parameter inference code, J. Cosmol. Astropart. Phys. 02 (2013) 001.

[45] T. Brinckmann and J. Lesgourgues, MontePython 3: boosted MCMC sampler and other features, Phys. Dark Universe **24,** 100260 (2019).

[46] J. Lesgourgues, The Cosmic Linear Anisotropy Solving System (CLASS) I: Overview, arXiv:1104.2932.

[47] D. Blas, J. Lesgourgues, and T. Tram, The Cosmic Linear Anisotropy Solving System (CLASS) II: Approximation schemes, J. Cosmol. Astropart. Phys. 07 (2011) 034.

[48] M. Zumalacrregui, E. Bellini, I. Sawicki, J. Lesgourgues, and P. G. Ferreira, hiclass: Horndeski in the Cosmic Linear Anisotropy Solving System, J. Cosmol. Astropart. Phys. 08 (2017) 019.

[49] E. Bellini, I. Sawicki, and M. Zumalacrregui, hiclass: Background Evolution, Initial Conditions and Approximation Schemes, J. Cosmol. Astropart. Phys. 02 (2020) 008.

[50] E. Bellini et al., Comparison of Einstein-Boltzmann solvers for testing general relativity, Phys. Rev. D **97,** 023520 (2018).

[51] A. Lewis, GetDist: a Python package for analysing Monte Carlo samples, arXiv:1910.13970.

[52] D. Paoletti, M. Braglia, F. Finelli, M. Ballardini, and C. Umilt, Isocurvature fluctuations in the effective Newton's constant, Phys. Dark Universe **25,** 100307 (2019).

[53] O. Pisanti, A. Cirillo, S. Esposito, F. Iocco, G. Mangano, G. Miele, and P. D. Serpico, PArthENoPE: Public Algorithm Evaluating the Nucleosynthesis of Primordial Elements, Comput. Phys. Commun. **178,** 956 (2008).

[54] N. Aghanim et al. (Planck Collaboration), Planck 2018 results. V. CMB power spectra and likelihoods, arXiv:1907.12875.

[55] Y. Akrami et al. (Planck Collaboration), Planck 2018 results. I. Overview and the cosmological legacy of Planck, arXiv:1807.06205.

[56] S. Alam et al. (BOSS Collaboration), The clustering of galaxies in the completed SDSS-III Baryon Oscillation Spectroscopic Survey: cosmological analysis of the DR12 galaxy sample, Mon. Not. R. Astron. Soc. **470,** 2617 (2017).

[57] A. J. Ross et al. (BOSS Collaboration), The clustering of galaxies in the completed SDSS-III Baryon Oscillation Spectroscopic Survey: Observational systematics and baryon acoustic oscillations in the correlation function, Mon. Not. R. Astron. Soc. **464,** 1168 (2017).

[58] M. Vargas-Magaa et al., The clustering of galaxies in the completed SDSS-III Baryon Oscillation Spectroscopic Survey: theoretical systematics and Baryon Acoustic Oscillations in the galaxy correlation function, Mon. Not. R. Astron. Soc. **477,** 1153 (2018).

[59] F. Beutler et al. (BOSS Collaboration), The clustering of galaxies in the completed SDSS-III Baryon Oscillation Spectroscopic Survey: baryon acoustic oscillations in the Fourier space, Mon. Not. R. Astron. Soc. **464,** 3409 (2017).

[60] F. Beutler, C. Blake, M. Colless, D. Jones, L. Staveley-Smith, L. Campbell, Q. Parker, W. Saunders, and F. Watson, The 6dF Galaxy Survey: Baryon Acoustic Oscillations and the Local Hubble Constant, Mon. Not. R. Astron. Soc. **416,** 3017 (2011).

[61] A. J. Ross, L. Samushia, C. Howlett, W. J. Percival, A. Burden, and M. Manera, The clustering of the SDSS DR7 main Galaxy sample–I. A 4 per cent distance measure at $z = 0.15$, Mon. Not. R. Astron. Soc. **449,** 835 (2015).

[62] C. D. Huang, A. G. Riess, W. Yuan, L. M. Macri, N. L. Zakamska, S. Casertano, P. A. Whitelock, S. L. Hoffmann, A. V. Filippenko, and D. Scolnic, Hubble Space Telescope Observations of Mira Variables in the Type Ia Supernova Host NGC 1559: An Alternative Candle to Measure the Hubble Constant, Astrophys. J. **889,** 5 (2020).

[63] M. J. Reid, J. A. Braatz, J. J. Condon, L. J. Greenhill, C. Henkel, and K. Y. Lo, The Megamaser Cosmology Project: I. VLBI observations of UGC 3789, Astrophys. J. **695,** 287 (2009).

[64] A. R. Liddle, Information criteria for astrophysical model selection, Mon. Not. R. Astron. Soc. **377,** L74 (2007).

[65] C. J. Copi, A. N. Davis, and L. M. Krauss, A New nucleosynthesis constraint on the variation of G, Phys. Rev. Lett. **92,** 171301 (2004).

[66] C. Bambi, M. Giannotti, and F. L. Villante, The Response of primordial abundances to a general modification of G(N) and/or of the early Universe expansion rate, Phys. Rev. D **71,** 123524 (2005).

[67] A. Coc, K. A. Olive, J. P. Uzan, and E. Vangioni, Big bang nucleosynthesis constraints on scalar-tensor theories of gravity, Phys. Rev. D **73,** 083525 (2006).

[68] E. Garcia-Berro, E. Gaztanaga, J. Isern, O. Benvenuto, and L. Althaus, On the evolution of cosmological type ia supernovae and the gravitational constant, arXiv:astro-ph/9907440.

[69] A. Riazuelo and J. P. Uzan, Cosmological observations in scalar - tensor quintessence, Phys. Rev. D **66,** 023525 (2002).

[70] S. Nesseris and L. Perivolaropoulos, Evolving newton's constant, extended gravity theories and snia data analysis, Phys. Rev. D **73,** 103511 (2006).

[71] B. S. Wright and B. Li, Type Ia supernovae, standardizable candles, and gravity, Phys. Rev. D **97,** 083505 (2018).

[72] D. M. Scolnic *et al.*, The complete light-curve sample of spectroscopically confirmed SNe Ia from Pan-STARRS1 and cosmological constraints from the combined pantheon sample, Astrophys. J. **859,** 101 (2018).

[73] H. Desmond, B. Jain, and J. Sakstein, Local resolution of the Hubble tension: The impact of screened fifth forces on the cosmic distance ladder, Phys. Rev. D **100,** 043537 (2019); **101,** 069904(E) (2020).

[74] H. Desmond and J. Sakstein, Screened fifth forces lower the TRGB-calibrated Hubble constant too, arXiv:2003.12876.

[75] S. Weinberg, Goldstone Bosons as Fractional Cosmic Neutrinos, Phys. Rev. Lett. **110,** 241301 (2013).

[76] G. Ballesteros, A. Notari, and F. Rompineve, The H_0 tension: ΔG_N vs. $\Delta N_{\rm eff}$, arXiv:2004.05049.